Segmentation and tracking of the left ventricle in 3D MRI sequences using an active surface model

Julien Mille, Romuald Boné, Pascal Makris, Hubert Cardot
Université François Rabelais de Tours, Laboratoire Informatique, Tours, France
{julien.mille, romuald.bone, pascal.makris, hubert.cardot}@univ-tours.fr

Abstract

We describe a 3D+T active surface model for segmentation and tracking of the left ventricular endocardium within 3D MRI sequences of the cardiac cycle. In order to perform segmentation and tracking simultaneously, the surface structure is divided through both time and space, and is therefore handled as an array of planar active contours, interconnected between adjacent slices and frames, providing spatial and temporal consistency. In a given frame, the stacking of slice contours constitute a 3D triangular mesh with a cylindrical topology. Extraction of ventricle border is performed by means of energy minimization, using a combination of boundary-based term and a new computationally efficient region-based term.

1 Introduction

The problem of human left ventricle (LV) segmentation and tracking in MRI data has been extensively addressed for the last two decades. Among relatively recent researches, several works are based on the well-known active contour model or "snake" by Kass *et al.* [4]. Using such models, LV endocardial and epicardial boundaries were tracked in 3D MRI sequences, starting from the estimated contour in an initial slice and propagating the contour to other frames and slices [3][10]. Implicit contours based on level sets were also used for LV segmentation [9] and tracking [7]. Significant work was done using the active shape models (ASM) [12]. In [5], the 3D boundary of endocardium and epicardium was recovered with an ASM-based triangular mesh.
Most of the above-cited works took 3D MRI sequences as input data, but did not use spatial and temporal correlation in these sequences to build a time-varying surface. Clearly, a dynamic 3D structure of the ventricle evolving through the cardiac cycle is a valuable feature for visualization. Moreover, the object of interest is often tracked sequentially, which may be prone to error propagation. The model should be designed in order to evolve freely in the whole sequence, taking advantage of temporal correlation. In addition, we believe that in the case of cardiac segmentation, explicit models should be privileged over their implicit counterparts, since the topology is known in advance.
Towards this goal, our 3D+T active surface performs segmentation and tracking simultaneously in a common optimization process, avoiding sequential tracking. The surface structure is divided through both time and space as an array of correlated planar active contours, each one adapting its geometry to local image features. In order to provide spatial and temporal consistency, the active contours are interconnected between adjacent slices and frames. In a given frame, the stacking of slice contours constitute a 3D triangular mesh with a cylindrical topology. Extraction of ventricle border is performed by means of energy minimization, including internal energy to guarantee spatial and temporal regularity of the surface, and external energy to drive the surface towards the endocardium. Low

contrast between neighboring anatomic structures, resulting in a blurred boundary between the blood pool and myocardium, and the presence of dark papillary muscles are the main difficulties encountered when dealing with cardiac MRI. To overcome the limitations of uniquely edge-based deformable models, our external energy includes a new region-based term, computed in a narrow band around the contour, ensuring computational efficiency.

2 Deformable model for segmentation and tracking

Given the input image sequence $I : \mathbb{R}^3 \times \Omega_\tau \to \mathbb{R}$, where $I(x, y, z, \tau)$ is the intensity of voxel (x, y, z) at time τ, we introduce the 3D+T deformable model $\mathbf{M} : \Omega_u \times \Omega_v \times \Omega_\tau \to \mathbb{R}^3$. Following the idea of Paragios [7], segmentation and tracking are solved simultaneously by evolving $\mathbf{M}$ in order to minimize the following energy:

$$E(\mathbf{M}) = \int_{\Omega_\tau} \int_{\Omega_v} E_{contour}(\mathbf{C}_{v,\tau}) dv d\tau + \omega_t E_t(\mathbf{M}) + \omega_s E_s(\mathbf{M}) \tag{1}$$

Due to the nature of the image sequence, the resolution in the z-dimension is much weaker than in other dimensions (data is sparsely sampled). This principle is depicted in fig. 1 (left), considering that the z-axis is vertical. Taking this discontinuity into account, we should avoid to interpolate, differentiate or integrate I with respect to z. To suit our deformable surface $\mathbf{M}$ to such kind of data, we adopt a cylindrical topology by putting $M_z(u, v, \tau) = h_z v$, where h_z is the resolution in the z-direction. At a given τ, the surface is a generalized cylinder which horizontal cross sections are closed curves. In the previous equation, $\mathbf{C}_{v,\tau} : \Omega_u \to \mathbb{R}^2$ is the cross section of $\mathbf{M}$ at a fixed v and τ, such that $\mathbf{M}(u, v, \tau) = (\mathbf{C}_{v,\tau}(u), h_z v)$. We separate terms related to 2D contours and terms related to the 3D and temporal regularization. The spatial regularization term E_s smoothes the surface in the z-direction.

$$E_s(\mathbf{M}) = \int_{\Omega_\tau} \int_{\Omega_v} \int_{\Omega_u} \left\| \frac{\partial^2 \mathbf{M}}{\partial v^2} \right\| du\ dv\ d\tau \tag{2}$$

The ventricle is a non-rigid object deforming with low and constant speed. This knowledge is embedded into the energy functional using an inertial term. One may note that we do not rely on a particular motion model. Our temporal regularization energy E_t involves the second order τ-derivative of the surface:

$$E_t(\mathbf{M}) = \int_{\Omega_\tau} \int_{\Omega_v} \int_{\Omega_u} \left\| \frac{\partial^2 \mathbf{M}}{\partial \tau^2} \right\| du\ dv\ d\tau \tag{3}$$

Weights ω_t and ω_s control the influence of the energies. Setting $\omega_t = \omega_s = 0$ would delete temporal and spatial regularity, causing the 3D+T surface to behave like a set of independently evolving 2D active contours. We now focus on the contour energy.

$$E_{contour}(\mathbf{C}) = \omega_c E_c(\mathbf{C}) + \omega_e E_e(\mathbf{C}) + \omega_r E_r(\mathbf{C}) \tag{4}$$

The internal energy E_c is the regularization term. We use the curvature

$$E_c(\mathbf{C}) = \int_{\Omega_u} \left\| \frac{\partial^2 \mathbf{C}}{\partial u^2} \right\| du \tag{5}$$

Omitting the first-order regularization term allows the contour to undergo large variations of its area. However, once discretized as a polygon, the contour needs to be periodically reparameterized to keep control points evenly spaced. The boundary term E_e makes the contour locate on salient edges of the image:

$$E_e(\mathbf{C}) = -\int_{\Omega_u} \|\nabla f(\mathbf{C}(u))\| du \tag{6}$$

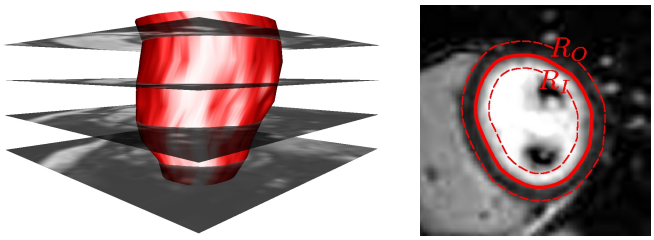

Figure 1. 3D deformable surface with cylindrical topology with crossing image slices (left) and 2D planar contour with inner and outer band domains for region-based energy (right)

where f is a 2D slice of sequence I, such that $f(x,y) = I(x,y,h_z v_0, \tau_0)$. Instead of computing the region term on the whole domain enclosed by $\mathbf{C}$ and its background, which would involve filling algorithms [2], we consider that the contour evolves in order to satisfy a region-based term E_r only in its vicinity, i.e. in an inner and outer band of constant thickness on each side of the curve (see right part of fig. 1). Ideally, the outer band of the contour minimizing the region energy should fit the myocardium. Let R_I and R_O be the inner and outer band domains, and $\mathcal{A}_I$ and $\mathcal{A}_O$ their respective areas. We maximize the mean intensity difference between the inner and outer band, given that the blood pool inside the ventricle is brighter than the outside:

$$E_r(\mathbf{C}) = \frac{1}{\mathcal{A}_O} \iint_{R_O} f(x,y)dxdy - \frac{1}{\mathcal{A}_I} \iint_{R_I} f(x,y)dxdy \tag{7}$$

To allow easy implementation, integrals of f over regions need to be simplified to line integrals over the contour. Let $\vec{\mathbf{n}}$ be the inward normal defined at every curve point. Denoting the constant band thickness B, region R_I is bounded by $\mathbf{C}$ and $\mathbf{C} + B\vec{\mathbf{n}}$, whereas R_O is bounded by $\mathbf{C}$ and $\mathbf{C} - B\vec{\mathbf{n}}$. Let us write our main simplification:

$$\iint_{R_I} f(x,y)dxdy \approx \int_0^B \int_{\Omega_u} f(\mathbf{C}+b\vec{\mathbf{n}}) \left\| \frac{d(\mathbf{C}+b\vec{\mathbf{n}})}{du} \right\| du\ db \tag{8}$$

and similarly for R_O, replacing $\vec{\mathbf{n}}$ by $-\vec{\mathbf{n}}$. Since the entire regions are not considered in the energy functional, they are not forced to verify an intensity homogeneity criterion. Homogeneity is usually not desirable for the backgound in real images. For the object, we should point out that the region energy is used to overcome issues raised by noise and weak edges, rather than seeking for a real region-based partition.

3 Implementation and energy minimization

Given an image sequence divided through time into T frames and through space (depth) into Z slices, the model is discretized as an array of active contours, each one being discretized as a polygon $[\mathbf{p}_1, \mathbf{p}_2, ..., \mathbf{p}_n]$. We denote $\mathbf{p}_{i,z,t}$ the i^{th} vertex of contour located in slice $z \in [1, Z]$ at frame $t \in [1, T]$. We denote $n_{z,t}$ the number of vertices in this contour, which varies as the curve is resampled during deformation. Any vertex belonging to slice z and frame t has connections to vertices in slices $z-1$ and $z+1$ (interslice connections, drawn with thick lines in fig.3), and in frames $t-1$ and $t+1$ (interframe connections, drawn with dashed lines in fig.3). These connections are handled through neighboring sets. We denote $\mathcal{S}^+_{i,z,t}$ and $\mathcal{S}^-_{i,z,t}$ the set of indices of neighbors connected to vertex $\mathbf{p}_{i,z,t}$ in slice $z+1$ and $z-1$, respectively. Similarly, we denote $\mathcal{F}^+_{i,z,t}$ and $\mathcal{F}^-_{i,z,t}$ the set of indices of

neighbors linked to vertex $\mathbf{p}_{i,z,t}$ in frames $t+1$ and $t-1$, respectively. At a given frame, the contours linked with interslice connections form a 3D triangular mesh [11]. The interframe connections are implemented for time regularization purpose, i.e. for the implementation of temporal energy E_t in eq. 1. The interslice connections do not only serve for spatial regularization but also for mesh visualization. Incidentally, the mesh representation is useful for quantitative analysis, such as volume estimation. To minimize the energy functional, the

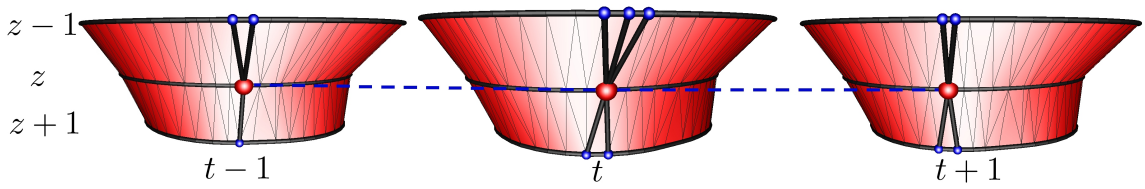

Figure 2. Interslice and interframe connections between vertices

contours are iteratively deformed using the greedy algorithm [13], consisting in successive local optimizations: at each iteration, a square window around each vertex $\mathbf{p}$ is considered. The energy is computed at each pixel $\tilde{\mathbf{p}}$ belonging to the window and the vertex is moved to the location leading to the lowest energy. Previous work [6] has shown that greedy algorithm performed faster than gradient descent methods for active contours and surfaces and led to better segmentation results. In order the greedy approach to be applicable, the energy is discretized and expressed as a sum of independent vertex energies.

$$E(\mathbf{M}) = \sum_{t=1}^{T} \sum_{z=1}^{Z} \sum_{i=1}^{n_{z,t}} E(\mathbf{p}_{i,z,t}) \tag{9}$$

All previously described energies are distributed among vertices. Thus, the energy of vertex $\mathbf{p}$ is expressed as follows:

$$E(\mathbf{p}) = \omega_c E_c(\mathbf{p}) + \omega_e E_e(\mathbf{p}) + \omega_r E_r(\mathbf{p}) + \omega_s E_s(\mathbf{p}) + \omega_t E_t(\mathbf{p}) \tag{10}$$

where E_c, E_e and E_r are the contour-related energies, independently computed within each slice, whereas E_s and E_t relate the vertex to its neighborhood in adjacent slices and frames. With a view to concision, we will omit reference to z and t for contour-related energies. The internal energy is an approximation of local curvature, which can be naturally expressed by the angle formed by $\mathbf{p}_i$ and its two neighbors, using dot product.

$$E_c(\tilde{\mathbf{p}}_i) = \frac{(\tilde{\mathbf{p}}_i - \mathbf{p}_{i-1}) \cdot (\tilde{\mathbf{p}}_i - \mathbf{p}_{i+1})}{\|\tilde{\mathbf{p}}_i - \mathbf{p}_{i-1}\| \, \|\tilde{\mathbf{p}}_i - \mathbf{p}_{i+1}\|} \tag{11}$$

Unlike discretization of the second-order derivative, this expression is independent of the spacing between vertices, making E_c less sensitive to sampling. The edge term $E_e(\tilde{\mathbf{p}}_i) = -\|\nabla f(\tilde{\mathbf{p}}_i)\|$ is computed using Sobel operator. The discrete region energy is based on equations 7 and 8, from which we removed the arc length element. Its minimization tends to move the vertex to the location giving brightest and darkest pixels in the inner and outer sides, respectively.

$$E_r(\tilde{\mathbf{p}}_i) = \sum_{b=1}^{B} f(\tilde{\mathbf{p}}_i - b\vec{\mathbf{n}}_i) - \sum_{b=0}^{B-1} f(\tilde{\mathbf{p}}_i + b\vec{\mathbf{n}}_i) \tag{12}$$

where $\vec{\mathbf{n}}_i$ is the inward unit normal vector, orthogonal to the approximated tangent. B is the constant band thickness. The interslice energy constrains the mesh to keep smoothly varying cross sections. It relates vertices to their neighbors in adjacent slices, in the same

manner that the curvature energy brings vertices closer to their neighbors within a slice.

$$E_s(\mathbf{p}_{i,z,t}) = \left\| \tilde{\mathbf{p}}_{i,z,t} - \frac{1}{2}\left(\frac{1}{\left|\mathcal{S}^+_{i,z,t}\right|} \sum_{j \in \mathcal{S}^+_{i,z,t}} \mathbf{p}_{j,z+1,t} + \frac{1}{\left|\mathcal{S}^-_{i,z,t}\right|} \sum_{j \in \mathcal{S}^-_{i,z,t}} \mathbf{p}_{j,z-1,t} \right) \right\| \quad (13)$$

where the term between brackets in the centroid of the interslice neighbors of vertex $\mathbf{p}_i$. Similarly, in order to maintain temporal smoothness, the interframe energy relates the vertex to its neighbors in adjacent frames of the same slice. Its expression is obtained by replacing $\mathcal{S}$ by $\mathcal{F}$ in the previous equation.

4 Experiments

We apply the proposed method on 3D MR cardiac sequences in short-axis view, divided into 25 phases and 9 slices covering the heart from apex to valves. Each slice is a 256×256 image with an approximative resolution of 2mm/pixel in the x and y directions and 9mm/pixel in the z direction (slice thickness is 9mm). Segmentation experiments are conducted on data where expert segmentation is available, so that segmentation quality can be assessed. The modified Hausdorff distance $\mathcal{H}_{mean}$ introduced in [1] is used to measure the average fitting of the surface to the real boundary, whereas the original Haussdorf distance $\mathcal{H}_{max}$ corresponds to the greatest error between the two boundaries, evaluated over all frames and slices. In all our experiments, the surfaces are initialized as thin cylinders inside the left ventricle and inflated until reaching the heart wall. In general, reaching the endocardium boundaries is a complex task due to the presence of papillary muscles, appearing as dark patches inside the bright blood area. We incorporate these muscles inside the surface thanks to topology control. When an active contour wraps around a papillary muscle, intersection between edges are detected and a topological change is performed [8], so that only the external curve is kept. This maintains a valid contour without self-intersection, topologically equivalent to a circle. Figure 3 shows segmentation results obtained on a normal heart. The three first rows depict to slices 1, 5 and 9, respectively. The last row is a 3D reconstruction of the triangular mesh. The smallest volume is observed at frame $t = 10$, which is the end-systolic phase. Distance values are $H_{mean} = 0.85$ and $H_{max} = 1.47$, corresponding to satisfactory segmentations.

5 Conclusion

We have described a 3D+T explicit deformable surface for segmentation and tracking of the endocardium in 3D MRI sequences. The model topology is well suited to sparsely sampled short axis acquisitions. The energy formulation ensured smoothness of the surface at a given time, but also through the cardiac cycle, allowing to perform segmentation and tracking with the same minimization process. From an initial location inside the heart, the surface fits to the ventricle wall boundaries thanks to a combination of edge-based and region-based features. We may consider a number of extension to this work. First, we plan to incorporate extra knowledge into the surface evolution process, in order to constrain its motion. Indeed, strong cardiac pathologies may affect the shape of the ventricle, in such a way that the surface fails at segmenting the endocardium precisely. For instance, shape priors could be employed in order not to confuse dark muscles with the myocardium. Moreover, various coupled surfaces with spatial relationships may be used to segment and track the epicardium as well as the right ventricle.

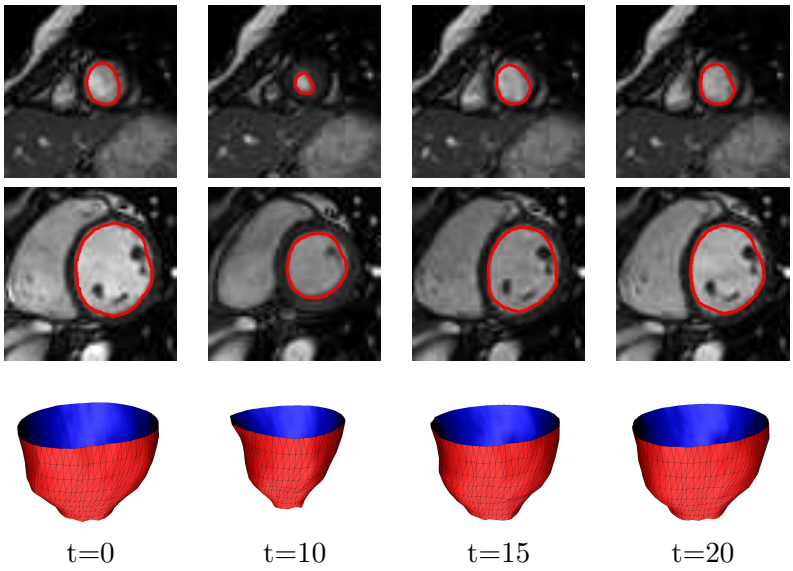

Figure 3. Segmentation results on normal heart. Slices 1, 5 and 9 (three upper rows) and triangular mesh representation (bottom row)

References

[1] M-P. Dubuisson and A.K. Jain. A modified Hausdorff distance for object matching. In 12^{th} *International Conference on Pattern Recognition (ICPR)*, pages 566–568, Jerusalem, Israel, 1994.

[2] J. Ivins and J. Porrill. Active region models for segmenting textures and colours. *Image and Vision Computing*, 13(5):431–438, 1995.

[3] M-P. Jolly, N. Duta, and G. Funka-Lea. Segmentation of the left ventricle in cardiac MR images. In *IEEE International Conference on Computer Vision (ICCV)*, volume 1, pages 501–508, Vancouver, Canada, 2001.

[4] M. Kass, A. Witkin, and D. Terzopoulos. Snakes: active contour models. *International Journal of Computer Vision*, 1(4):321–331, 1988.

[5] M.R. Kaus, J. Von Berg, J. Weese, W. Niessen, and V. Pekar. Automated segmentation of the left ventricle in cardiac MRI. *Medical Image Analysis*, 8(3):245–254, 2004.

[6] J. Mille, R. Boné, P. Makris, and H. Cardot. Greedy algorithm and physics-based method for active contours and surfaces: a comparative study. In *IEEE International Conference on Image Processing (ICIP)*, pages 1645–1648, Atlanta, USA, 2006.

[7] N. Paragios. A level set approach for shape-driven segmentation and tracking of the left ventricle. *IEEE Transactions on Medical Imaging*, 22(6):773–776, 2003.

[8] A. Perera, C-L. Tsai, R. Flatland, and C. Stewart. Maintaining valid topology with active contours: theory and application. In *IEEE International Conference on Computer Vision and Pattern Recognition (CVPR)*, pages 1496–1502, Hilton Head, SC, USA, 2000.

[9] C. Pluempitiwiriyawej, J. Moura, Y-J. Wu, and C. Ho. STACS: New active contour scheme for cardiac MR image segmentation. *IEEE Transactions on Medical Imaging*, 24(5):593–603, 2005.

[10] I-H. Shin, M-J. Kwon, S-T. Chung, and H.W. Park. Segmentation and visualization of left ventricle in MR cardiac images. In *IEEE International Conference on Image Processing (ICIP)*, volume 2, pages 89–92, Rochester, New York, USA, 2002.

[11] G. Slabaugh and G. Unal. Active polyhedron: surface evolution theory applied to deformable meshes. In *IEEE Computer Vision and Pattern Recognition (CVPR)*, volume 2, pages 84–91, San Diego, USA, 2005.

[12] H. van Assen, M. Danilouchkine, A. Frangi, S. Ordás, J. Westenberg, J. Reiber, and B. Lelieveldt. SPASM: A 3D-ASM for segmentation of sparse and arbitrarily oriented cardiac MRI images. *Medical Image Analysis*, 10(2):286–303, 2006.

[13] D.J. Williams and M. Shah. A fast algorithm for active contours and curvature estimation. *Computer Vision, Graphics, and Image Processing: Image Understanding*, 55(1):14–26, 1992.